Petroleum Science 21 (2024) 410–429

Contents lists available at ScienceDirect

Petroleum Science

journal homepage: www.keaipublishing.com/en/journals/petroleum-science

Original Paper

Insights into *in-situ* imbibition behavior of fracturing fluid in propped shale fractures based on nuclear magnetic resonance: A case study from Longmaxi Formation shale, Sichuan Basin, China

Jing-Jing Guo*, Kai-Xiang Di, Lie-Hui Zhang**, Yu-Long Zhao, Hui-Ying Tang, Rui-Han Zhang, Ye Tian

National Key Laboratory of Oil and Gas Reservoir Geology and Exploitation, Southwest Petroleum University, Chengdu, 610500, Sichuan, China

ARTICLE INFO

Article history:
Received 14 April 2023
Received in revised form
18 September 2023
Accepted 26 September 2023
Available online 28 September 2023

Edited by Yan-Hua Sun

Keywords:
Forced imbibition
Migration
Soaking
NMR T_2 spectra
Propped fracture
Permeability recovery

ABSTRACT

Shale gas is an important component of unconventional oil and gas resources. Studying the imbibition behavior is helpful to optimize flowback parameters and enhance gas recovery. Recent imbibition studies have focused on shale matrix, and the pressure conditions discussed were mostly atmospheric. The initial imbibition behavior begins from propped fractures to matrix, but there are few studies working on explaining the imbibition behavior in propped fractures or the phenomenon of many shale wells exhibit higher productivity after a "soaking" period. Therefore, propped fracture samples were designed for imbibition and migration experiments. In order to accurately study the mechanism and main influencing factors of fracturing fluid imbibition and migration in propped and unpropped shale fractures under high temperature and high pressure, a series of experiments based on nuclear magnetic resonance (NMR) were carried out. Results showed that NMR T_2 spectra of all samples exhibited a bimodal distribution. The final imbibition volume of fracturing fluid was positively related to pressure and fracture width. The imbibition effect of fracturing fluid was more evident in matrix pores under high pressure. In the migration during soaking stage, the fracturing fluid gradually migrated from large pores to small pores and gradually displaced the shale gas from the matrix, thus allowing the water blocking in propped fractures to self-unlock to some extent. Gas permeability decreased in the imbibition stage, while it recovered in the migration stage to some extent.
© 2024 The Authors. Publishing services by Elsevier B.V. on behalf of KeAi Communications Co. Ltd. This is an open access article under the CC BY-NC-ND license (http://creativecommons.org/licenses/by-nc-nd/4.0/).

1. Introduction

Playing an important role in unconventional hydrocarbon resources, shale gas has received wide attention and publicity from the energy sector due to its huge geological reserves and considerable development prospects (Zou et al., 2021). The marine shale typically has a low porosity and ultra-low permeability, leading to an extremely limited seepage capacity. Hence, fracturing has become an important and effective means to improve its permeability and production. Currently, the fracturing fluid used in the field is mainly water-based. The flowback ratio of the fracturing fluid in reservoir optimization and subsequent development is basically below 30% (Shen et al., 2017). As a result, a large amount of fracturing fluid is detained in the reservoir and cannot flowback. Imbibition caused by high capillary force in micropores is the main mechanism of fracturing fluid retention and a key factor affecting shale reservoir productivity.

Many researchers have studied the imbibition behavior of porous media. Lucas (1918) first studied the spontaneous imbibition of a single capillary. Sherman and Holditch (1991) found that reservoir physical properties are significantly affected by fluids during fracturing, especially water phase trapping, resulting in significant reservoir damage. Bennion et al. (1996) conducted a detailed study of the mechanism of water phase trapping. Cluff and Byrnes (2010) found that fluid trapped in the reservoir affects the gas phase permeability of fractures by blocking the contact area between the fracture network and the matrix. Many researchers also completed the derivation using theoretical models of capillary

* Corresponding author.
** Corresponding author.
E-mail addresses: guojingjing@swpu.edu.cn (J.-J. Guo), zhangliehui@vip163.com (L.-H. Zhang).

https://doi.org/10.1016/j.petsci.2023.09.023
1995-8226/© 2024 The Authors. Publishing services by Elsevier B.V. on behalf of KeAi Communications Co. Ltd. This is an open access article under the CC BY-NC-ND license (http://creativecommons.org/licenses/by-nc-nd/4.0/).

force (Cai, 2021), such as Washburn's (LW) wet phase liquid self-imbibition model (Washburn, 1921), and Handy's gas-water self-imbibition model (Handy, 1960), and Terzaghi's model (Terzaghi, 1943). Corrections and extended studies were also conducted on this basis.

In terms of experiments, the direct weighing method (Ghanbari and Dehghanpour, 2015; Xia et al., 2021) and volume method were adopted to investigate the imbibition behavior of reservoir rocks. Gao et al. (2013) studied the hydration and water absorption effects of different fluids on shale powder and core samples at room temperature and pressure by volume method. Yang et al. (2017) compared the effect of self-imbibing of distilled water on shale and sandstone samples under normal temperature and pressure by direct weighing method, and they established a model to describe the relationship between ion diffusion and self-imbibition. However, most of the imbibition experiments were carried out based on spontaneous imbibition under room temperature and relatively low pressure. Only a few researchers studied the influence of confining pressure. Roshan et al. (2015) concluded that water phase imbibition of shale under confining pressure can still generate induced fractures. Zhu and Li (2021) combined the gravimetric method and nuclear magnetic resonance (NMR) technology to study the imbibition characteristics of different fluids in shale under low pressure. The studies of high confining pressure are relatively less, and most shale imbibition experiments were conducted on shale matrix samples, while only a few studies focused on the imbibition of shale propped fractures.

Moreover, fast flowback procedure sometimes cannot be achieved. Long-time interactions between fracturing fluid and shales may cause the redistribution of fracturing fluid in reservoirs and thus affect production capacity (Bazin et al., 2010; Cheng, 2012). In the field practice, quite a portion of shale wells exhibit higher productivity after a “soaking” period (referring to a period of well shut-in after hydraulic fracturing) (Bostrom et al., 2014; Wang and Rahman, 2015; Dutta et al., 2014; Mianmo et al., 2015). However, only a few research conclusions can be adopted to explain this phenomenon (Zeng et al., 2022), and current studies mostly focused on matrix samples but less on propped fracture samples.

Rock samples from Longmaxi Formation in Sichuan Basin were collected to conduct *in-situ* imbibition experiments under high pressure (30 and 60 MPa) and high temperature (110 °C). NMR T_2 spectrum responses were obtained during the imbibition and migration process. The distribution and migration of imbibed fracturing fluid in fractured shale and the seepage capacity alteration were also analyzed.

2. Methodology

2.1. Imbibition and migration in propped fractures

After hydraulic fracturing, the fractures filled with proppant constitute the main flowing space of shale gas. Under the influence of capillary force, osmotic pressure and other mechanisms, the fracturing fluid is gradually imbibed to the shale reservoir and continuously increases the volume of fluid in the reservoir. This process is considered as the imbibition during fracturing. Compared with the unpropped fracture, the propped fracture may provide more space for fluid imbibition.

After fracturing, there is often a shut-in period. A large amount of fracturing fluid retained in propped fractures would migrate from fractures to the shale matrix. Different from the previous imbibition stage, the total volume of fracturing fluid during this stage is constant. Fracturing fluid is redistributed in different pores in the reservoir after migration. This period is considered as migration during soaking stage.

Imbibition and migration experiments of fracturing fluid in propped fractures (Chen et al., 2020) with different widths were designed to explore the imbibition and migration behavior of fracturing fluid in fractures and matrices under various formation conditions. For propped fractures, the relationship between a specified fracture width and corresponding proppant placement concentration can be expressed as

$$D_f = \frac{c}{\rho} \tag{1}$$

$$M_s = dLc \tag{2}$$

where D_f is the propped fracture width, mm; c is the proppant placement concentration, g/mm^2; and ρ is the proppant volume density which is set as 0.0025 according to the field data, g/mm^3; M_s is the weight of proppant, g; d and L represent the diameter and length of the core plug sample, respectively, mm.

2.2. Theory of low-field NMR

NMR technology allows us to investigate the pore size distribution of rock samples. Pore size, surface properties and fluid properties are the main factors affecting the relaxation time in the NMR process (Saidian and Prasad, 2015). There are three relaxation mechanisms in the NMR process which are bulk relaxation, surface relaxation, and diffusion relaxation (Coates et al., 1999). If the fast diffusion condition is satisfied, the total relaxation rate of porous media is equal to the sum of individual relaxation rates.

The transverse relaxation time (T_2) can be expressed as

$$\left(\frac{1}{T_2}\right)_{\text{total}} = \left(\frac{1}{T_2}\right)_B + \left(\frac{1}{T_2}\right)_S + \left(\frac{1}{T_2}\right)_D \tag{3}$$

where $(1/T_2)_B$, $(1/T_2)_S$, and $(1/T_2)_D$ indicate the bulk, surface, and diffusion relaxation times, respectively, ms. $(1/T_2)_B$ reflects the relaxation properties of the fluid itself. $(1/T_2)_S$ reflects the influence of rock particle surface on relaxation process. $(1/T_2)_D$ reflects some fluids will exhibit obvious diffusion relaxation properties in CPMG pulse train with long echo intervals.

The surface relaxation time of rock samples, $(1/T_2)_S$, can be expressed as

$$\left(\frac{1}{T_2}\right)_S = \rho_2 \left(\frac{S}{V}\right)_{\text{pore}} \tag{4}$$

where ρ_2 is the surface relaxivity, μm/ms; $(S/V)_{\text{pore}}$ is the ratio of surface to volume of the pores filled with the ^{1}H containing fluid; $(S/V)_{\text{pore}}$ is a function of pore radius, which can be expressed as

$$\left(\frac{S}{V}\right)_{\text{pore}} = \frac{F_S}{r} \tag{5}$$

where F_S is the shape factor, dimensionless; r is pore radius, μm.

The diffusion relaxation time of rock samples, $(1/T_2)_D$, can be expressed as

$$\left(\frac{1}{T_2}\right)_D = \frac{D(\gamma G T_E)^2}{12} \tag{6}$$

where D is the molecular diffusion coefficient; γ is the gyromagnetic ratio of the ^{1}H proton; G is the field-strength gradient; and T_E is the inter-echo spacing used in the Carr-Purcell-Meiboom-Gill (CPMG) pulse sequences.

Given that T_E is extremely small in a homogeneous internal field

gradient, the value of $(1/T_2)_D$ is always negligible (Liu, 2017). Besides, T_{2B} is larger than T_{2S} for liquid in porous media, so that the value of $(1/T_2)_B$ can be ignored. The relaxation time (T_2) in Eq. (2) can be simplified as

$$T_2 \approx \frac{1}{\rho_2 F_S} \cdot r = C \cdot r \tag{7}$$

Eq. (7) indicates that the distribution of T_2 can be converted into the pore size distribution of the porous rock sample.

3. Materials and experiments

3.1. Shale sample preparation

Shale core samples collected from the Lower Silurian Longmaxi Formation in southern Sichuan Basin in China were prepared for subsampling for fracturing fluid imbibition and migration experiments. X-ray diffraction analysis and rock pyrolysis analysis were performed to obtain the mineral composition and total organic carbon (TOC) of the samples. Corresponding results were averaged and shown in Table 1.

The formula of the low-viscosity slickwater fracturing fluid used in this experiment is 0.2% drag reducer, 0.1% discharge aid and 0.05% fungicide. The ratio of emulsion to distilled water is 1:1000. The fracturing fluid density is 1.03 g/cm^3.

To investigate the imbibition and migration behavior in propped fractures, the shale plug samples were then prepared as follows (Fig. 1).

(1) An artificial fracture was created by Brazilian splitting.
(2) Quartz sand-ceramsite mixed proppant was prepared according to actual field data. The particle size of ceramsite was 40/70 mesh with 55% mass fraction, and the particle size of quartz sand was 70/140 mesh with 45% mass fraction.
(3) The proppant was uniformly placed on the fracture surface, and the top and bottom of the core were then sealed with 200 mesh non-magnetic gauze. The core was wrapped in heat-shrinkable tubes to ensure that the proppant will not leak.
(4) The widths of the propped fractures considered in the experiment were 0, 0.8, 1, 2, and 4 mm. For each fracture width, two series of samples were prepared.
(5) All samples were dried at 85 °C for at least 48 h to ensure that moisture was removed prior to the imbibition test.

The basic properties of the shale samples are shown in Table 2. Two groups of experiments were designed and conducted in this work. Group-I is designed to explore the imbibition and migration behavior of the propped fractures, and Group-II is designed to explore the seepage capacity alteration after imbibition. Initial gas porosity and permeability of all the samples were measured by the SCMS-H2 automatic core measurement system. The confining pressure is 5 MPa, and the pore pressure is 2 MPa when measuring the gas permeability of the prepared samples. It should be noted that the fracture widths shown in Table 2 are the designed widths. The actual widths measured after sample preparation and corresponding error are shown in Table 3. It is shown that the errors of the fracture width for all samples are less than 5%, indicating that the core sample preparation is acceptable. In order to facilitate understanding and analysis, the designed fracture width will be used in the subsequent analysis.

Table 1
Average mineral composition and TOC of shale samples.

Sample	Mineral component, wt%						TOC, wt%
	Quartz	Feldspar	Calcite	Dolomite	Pyrite	Clays	
Shale sample	42.6	10.3	7.3	9.2	1.2	29.4	3.77

Fig. 1. Propped fracture samples after being dried in a drying oven. Designed fracture widths are 0, 0.8, 1, 2, and 4 mm from left to right.

3.2. Wettability evaluation

Rock wettability is a very important property that affects the fluid distribution in rock pores, as well as the imbibition behavior of fracturing fluid in shales. Therefore, the contact angle of fracturing fluid on core surface is measured in this study. After the core was dried for 48 h, four representative shale matrix samples were selected, and the contact angle between the fracturing fluid and the core surface in the air was measured by a wetting angle measuring meter SDC-350 (a high-power microscope) at 28 °C and 101.3 kPa.

3.3. Experimental set-up for imbibition measurements

The experimental set-up for imbibition measurements consists of an automatic core measuring system, a high-pressure core holder, two pressure meters, three high-pressure syringe pump systems (confining pressure pump, displacement pump, and backpressure pump), a drying oven, a NMR instrument, and a data collection system (Fig. 2). The process of imbibition experiment was monitored by NMR spectrometer with a frequency of 2–30 MHz, 0.3 T magnetic intensity and 70 mm diameter magnetic coil. T_2 spectrum was measured using the CPMG pulse sequences generated from the inverse Laplace non-negative least square fitting of echo train data (Liu et al., 2020).

3.4. Procedure for imbibition and migration

The schematic of imbibition and migration experiment is shown in Fig. 3. The T_2 spectrum measurement reveal the imbibition volume and distribution of fracturing fluid in shale samples. The reservoir temperature of the deep marine shale gas reservoirs is about 110 °C, and the initial reservoir pressure is about 70–80 MPa. Considering the actual reservoir condition, the limitations of the experimental equipment and experiment safety, 30 MPa (or 60 MPa) and 110 °C were chosen as the experimental conditions.

Experimental procedures for experiment Group-I are as follows.

(1) Measure and record the weight, initial porosity and permeability of each sample after drying, and conduct NMR measurement to get the basic T_2 spectrum of the dry sample.
(2) Put the experimental core sample into the intermediate container. The intermediate container was filled with the fracturing fluid, and the pressure and the temperature of the

Table 2
Basic properties of shale samples.

Core ID	Weight, g	Length, mm	Diameter, mm	Porosity, %	Permeability, mD	Designed width, mm	Proppant concentration, g/mm^2
I-30-0	61.90	50.24	25.78	2.48	70	0	0
I-30-1	62.56	50.36	25.27	6.27	344	0.8	0.002
I-30-2	67.60	50.29	25.16	6.75	394	1	0.0025
I-30-3	59.42	51.30	25.34	10.33	784	2	0.005
I-30-4	58.44	51.36	25.14	12.14	1540	4	0.01
I-60-0	65.69	50.30	25.48	3.11	77	0	0
I-60-1	63.88	50.45	25.22	5.99	540	0.8	0.002
I-60-2	54.18	50.38	25.31	7.17	600	1	0.0025
I-60-3	60.56	51.08	25.58	9.77	925	2	0.005
I-60-4	58.72	52.12	25.36	13.56	1659	4	0.01
II-30-1	60.37	50.63	26.77	4.67	68	0	0
II-30-2	63.37	51.13	25.88	8.27	293	1	0.0025
II-30-3	61.08	51.40	25.43	10.52	745	2	0.005
II-30-4	59.10	48.61	25.95	14.27	916	4	0.01
II-60-1	61.44	52.18	26.31	5.17	88	0	0
II-60-2	62.88	51.38	26.11	7.98	375	1	0.0025
II-60-3	60.17	52.88	25.48	11.66	886	2	0.005
II-60-4	58.79	49.88	25.16	16.88	1027	4	0.01

Table 3
Fracture width error of shale samples.

Core ID	Designed width, mm	Actual width, mm	Error, %
I-30-0	0	0	0
I-30-1	0.8	0.77	3.75
I-30-2	1	1.05	5.00
I-30-3	2	1.92	4.00
I-30-4	4	3.85	3.75
I-60-0	0	0	0
I-60-1	0.8	0.83	3.75
I-60-2	1	1.02	2.00
I-60-3	2	2.08	4.00
I-60-4	4	3.95	1.25
II-30-1	0	0	0
II-30-2	1	0.98	2.00
II-30-3	2	1.94	3.00
II-30-4	4	3.81	4.75
II-60-1	0	0	0
II-60-2	1	1.03	2.00
II-60-3	2	2.09	4.50
II-60-4	4	3.87	3.25

intermediate container were set as 30 MPa (or 60 MPa) and 110 °C to simulate *in-situ* forced imbibition. Both ends of the core samples can fully contact with the fracturing fluid.

(3) At the 24th hour (1 day), 120th hour (5 days), and 168th hour (7 days) of the imbibition process, the core sample was taken from the intermediate container and then put into the non-magnetic core holder. Then slowly cycle up the pressure (by fluorocarbon oil) of the core holder to 30 MPa (or 60 MPa) under the temperature of 110 °C, and conduct NMR T_2 spectrum measurements. The parameters were set as follows: the waiting time set as 5000 ms, echo spacing set as 0.15 ms, number of echoes set as 4096, and the number of scans set as 64.

(4) After the 168-h forced imbibition experiment, the experimental core sample was then put into the drying oven at 60 °C for 20 min. The purpose of this procedure is to obtain a certain water saturation of the sample to simulate the water saturation around hydraulic fractures in the "soak" period after fracturing.

(5) According to field practice, the total water content in the shale reservoirs is constant during the "soak" period. To simulate this condition, the experimental sample was tightly wrapped to prevent moisture loss before the following migration experiment. Then put the wrapped sample into the core holder again, and gradually increase the inlet and outlet pressures of the core holder to 30 and 60 MPa by helium. The temperature of the experimental system was also set as 110 °C.

(6) During the migration process, conduct the NMR T_2 spectrum measurements at the 48th hour (2 days), 96th hour (4 days), and 144th hour (6 days).

Experimental procedures for experiment Group-II are as follows:

Steps (1)–(4) are the same as Group-I.

(5) The experimental sample was tightly wrapped and put into the core holder again, and measure the gas permeability of the sample with a certain water saturation. Then gradually increase the inlet and outlet pressures of the core holder to 30 and 60 MPa, and the temperature of the experimental system for migration tests was also set as 110 °C.

(6) During the migration process, measure the gas permeability of the core sample at the 48th hour (2 days), 96th hour (4 days), and 144th hour (6 days).

3.5. High-pressure mercury intrusion (HPMI) test

HPMI experiment was carried out on shale sample that taken from the same shale block, the sample was cut into small pieces and dried at 85 °C for 12 h before testing. The instrument can theoretically measure the pore size distribution from 3.6 nm to 1000 μm at the pressure of 60000 psia.

4. Results and discussion

In this study, the NMR T_2 spectra during imbibition and migration processes were analyzed to investigate the mechanisms of fracturing fluid imbibition, migration and redistribution in shales. Under constant temperature, pressure and fracture width were found to be the main factors affecting the imbibition dynamic and redistribution of fracturing fluid.

4.1. Contact angle

The contact angels for the analyzed shale samples are illustrated in Fig. 4. It can be observed that the contract angles of the samples

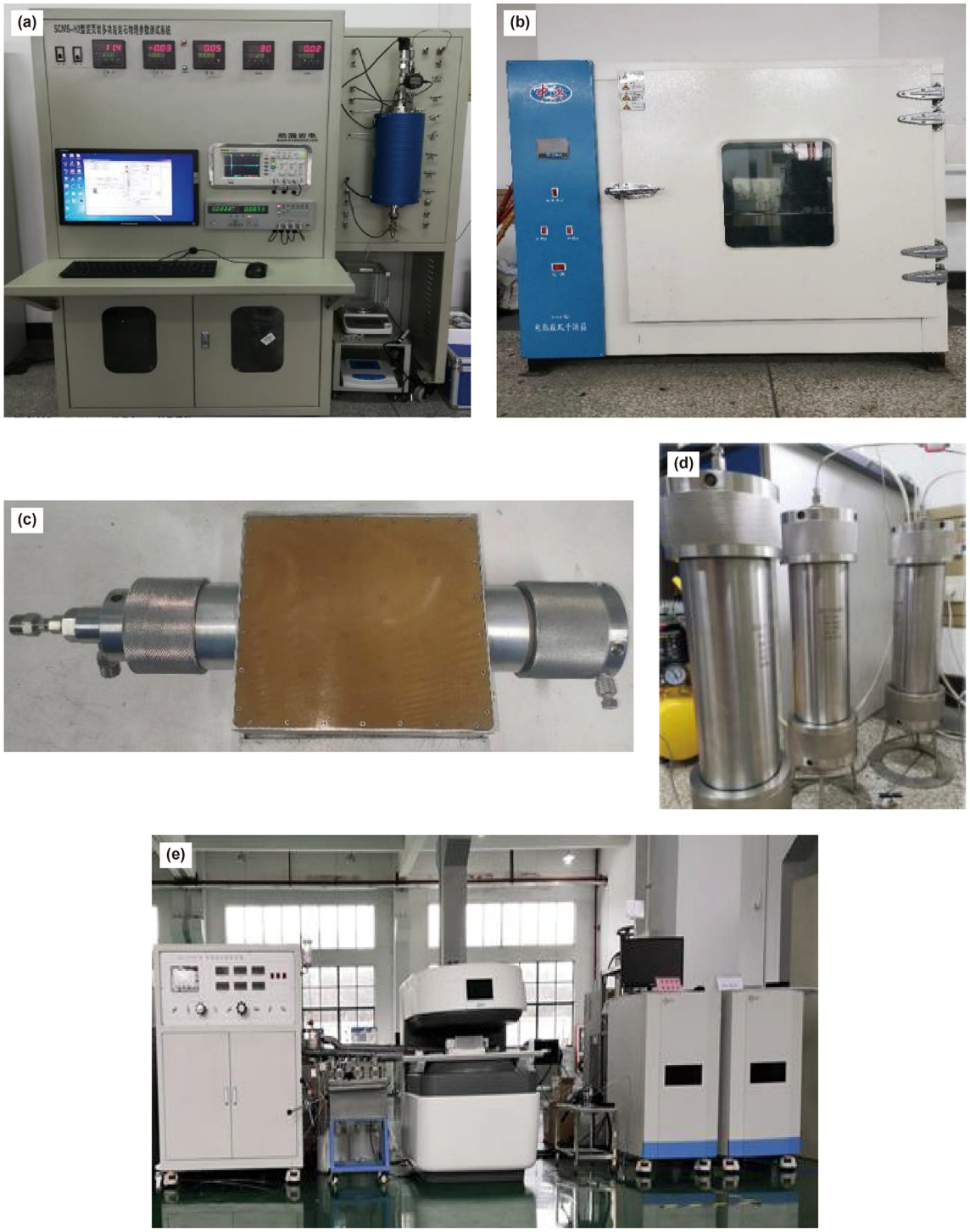

Fig. 2. Experimental set-up for high-pressure imbibition measurements. (**a**) SCMS-H2 automatic core measurement system used for porosity and permeability measurements; (**b**) Drying oven used for moisture removal and to provide a high-temperature experimental environment as designed; (**c**) High-pressure core holder; (**d**) High-pressure intermediate container; (**e**) MacroMR12-150H–I low-field NMR analysis and the imaging system used for the nondestructive measurement of hydrogen fluid distribution in core samples.

are between 73° and 83°, indicating that the experimental samples are water-wet.

4.2. Division of imbibition stages

The change of imbibition quantity for different core samples is shown in Fig. 5 and Table 4. The experimental results show that the imbibition process of shale samples with propped fracture can be divided into three stages: rapid imbibition in the early stage, transitional imbibition in the middle stage, and stable imbibition in the late stage.

The initial rapid imbibition stage can be observed on the 1st day (0–22 h), during which the imbibition volume of each sample increased rapidly and reached 86.24% on average of the final

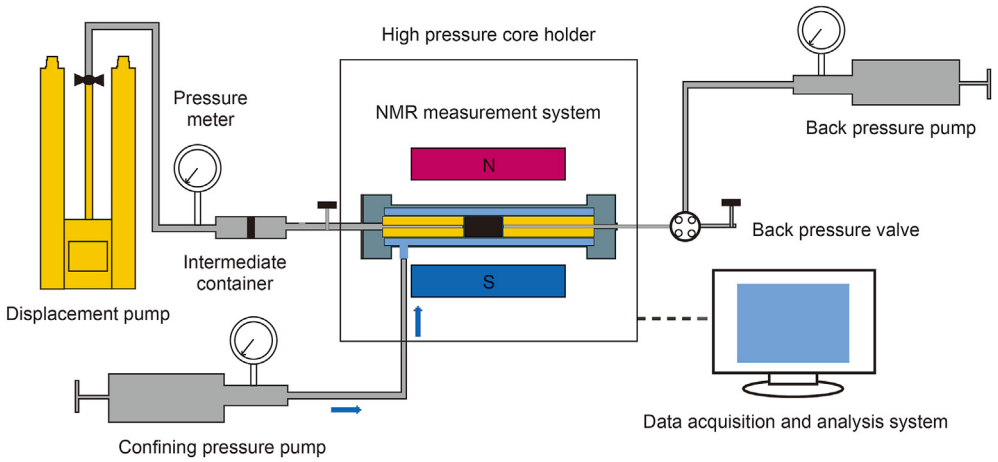

Fig. 3. Schematic of NMR-monitored imbibition and migration experiments.

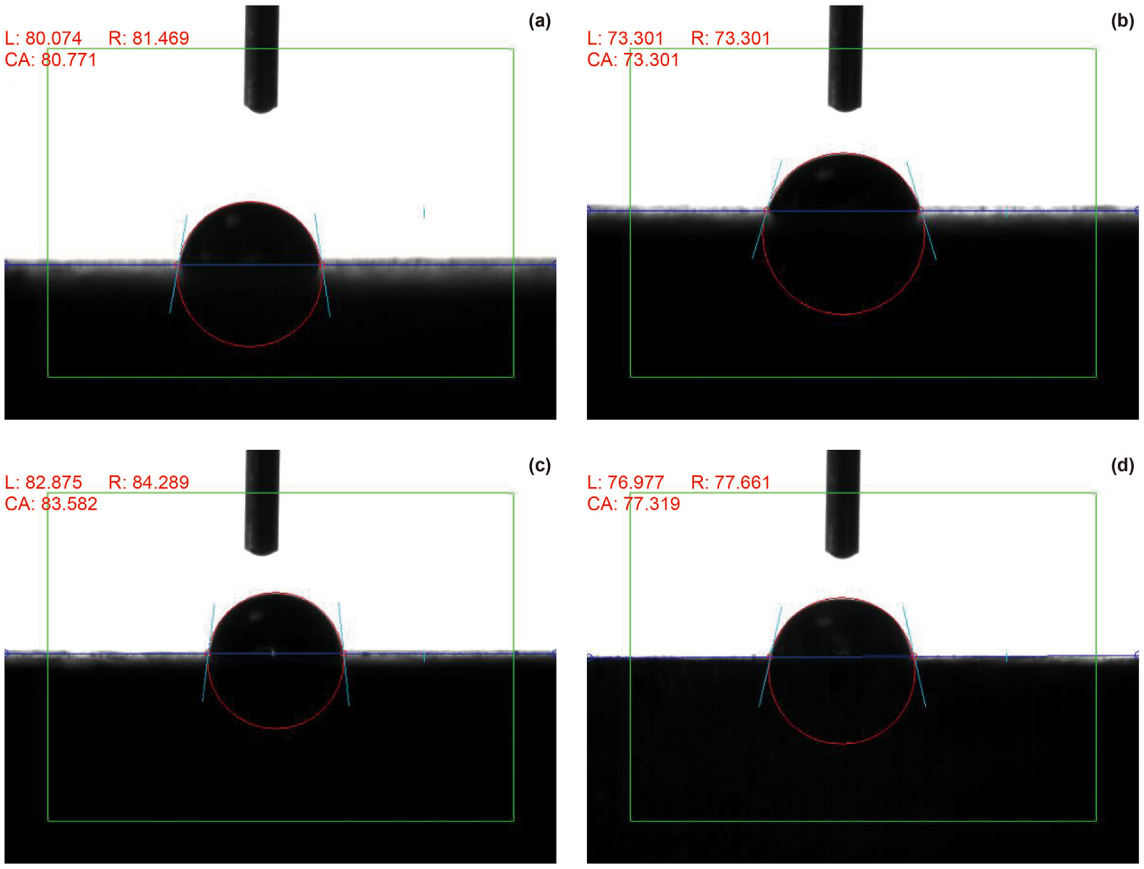

Fig. 4. Contract angle of shale samples.

imbibition volume at the 22nd hour. The duration of the initial rapid imbibition stage is basically the same under high-pressure imbibition and spontaneous imbibition (Zhu and Li, 2021). The 2nd day (22–48 h) can be considered as the middle transitional imbibition stage. The growth rate of imbibition quantity slowed down significantly. At the end of this stage, the imbibition volume reached about 96.19% on average of the final imbibition volume, which is 9.95% higher than that of the previous stage. Compared with spontaneous imbibition, the duration of the middle transitional imbibition stage of forced imbibition is relatively short. The imbibition process after 48 h can be considered as the late stable imbibition stage. This stage had the longest time span, and the imbibition quantity was basically stable (Fig. 5).

Table 4 shows the imbibition quantity for different core samples during different imbibition stages. It can be seen that for samples with the same fracture width, the total imbibition quantity of the fracturing fluid increased with imbibition pressure. For the propped fractures, as the pressure increased from 30 to 60 MPa, the increase ratio of the final imbibition quantity for samples with same fracture width was 15.06%–32.59%. The imbibition rate was then calculated

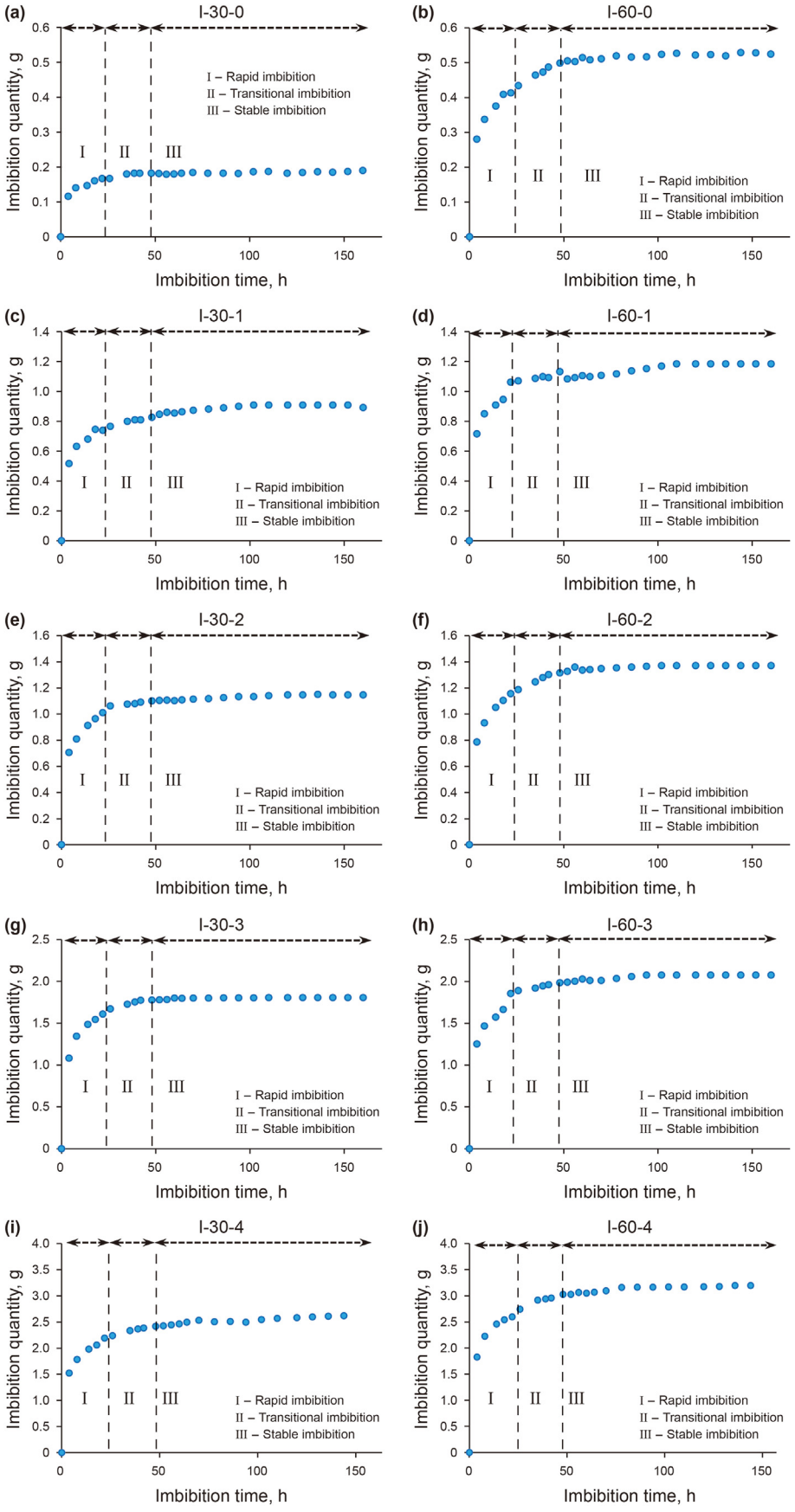

Fig. 5. Relationship between imbibition quantity and imbibition time.

Table 4
Cumulative imbibition quantity in each stage.

Core ID	Imbibition pressure, MPa	Fracture width, mm	Imbibition quantity, g		
			Stage I	Stage II	Stage III
I-30-0	30	0	0.167	0.182	0.190
I-60-0	60	0	0.413	0.499	0.525
I-30-1	30	0.77	0.740	0.827	0.893
I-60-1	60	0.83	1.061	1.133	1.184
I-30-2	30	1.05	1.010	1.101	1.147
I-60-2	60	1.02	1.157	1.314	1.370
I-30-3	30	1.92	1.608	1.777	1.806
I-60-3	60	2.08	1.857	1.986	2.078
I-30-4	30	3.85	2.192	2.417	2.628
I-60-4	60	3.95	2.597	3.023	3.198

according to imbibition quantity in different times (Fig. 6(a)). For the same fracture width, the imbibition rate at 60 MPa was generally higher than that at 30 MPa.

It can be concluded that pressure showed a significant effect on imbibition quantity and imbibition rate. Under high pressure, the fracturing fluid can more easily invade the micro-pores and throats in shale samples around the hydraulic fractures. Therefore, it may cause a considerable error if one uses the imbibition behavior obtained from low-pressure imbibition or spontaneous imbibition experiments to describe the *in-situ* imbibition effect in deep shale

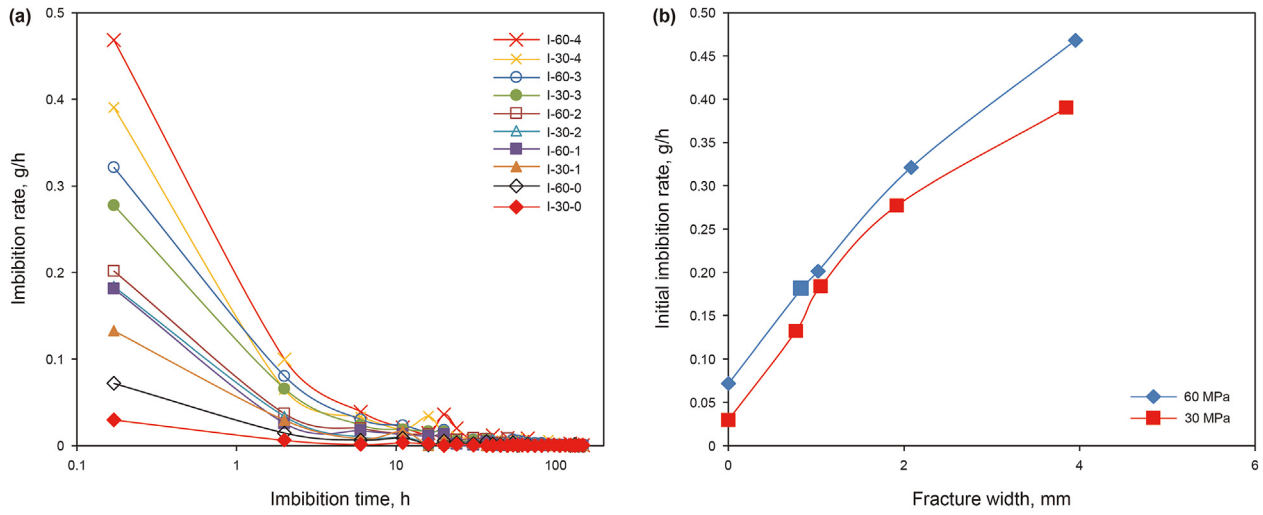

Fig. 6. Imbibition rate of shale core samples. (**a**) Imbibition rate at different stages; (**b**) Initial imbibition rate.

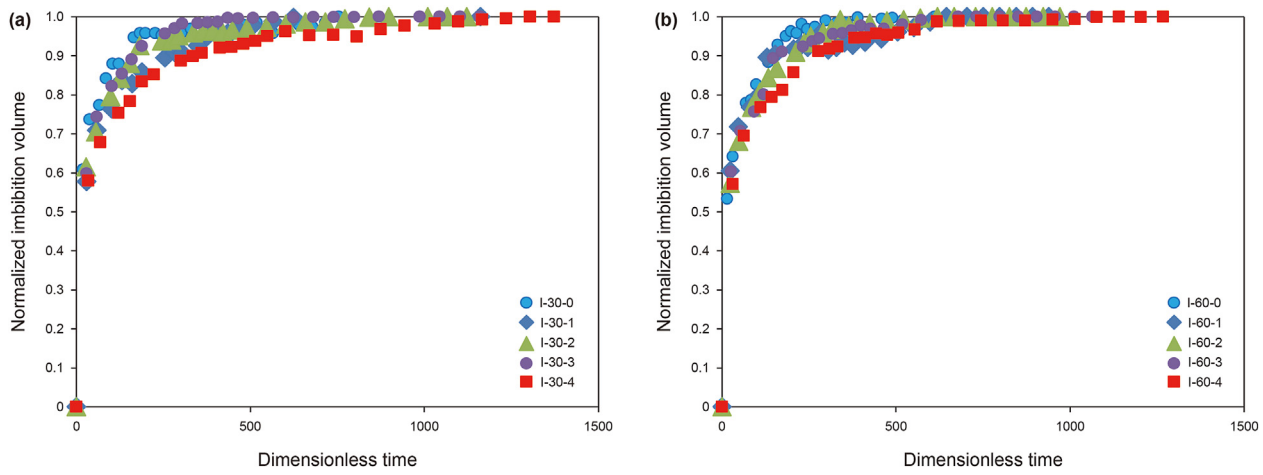

Fig. 7. Correlation between normalized imbibition volume and dimensionless time at different pressures. (**a**) 30 MPa; (**b**) 60 MPa.

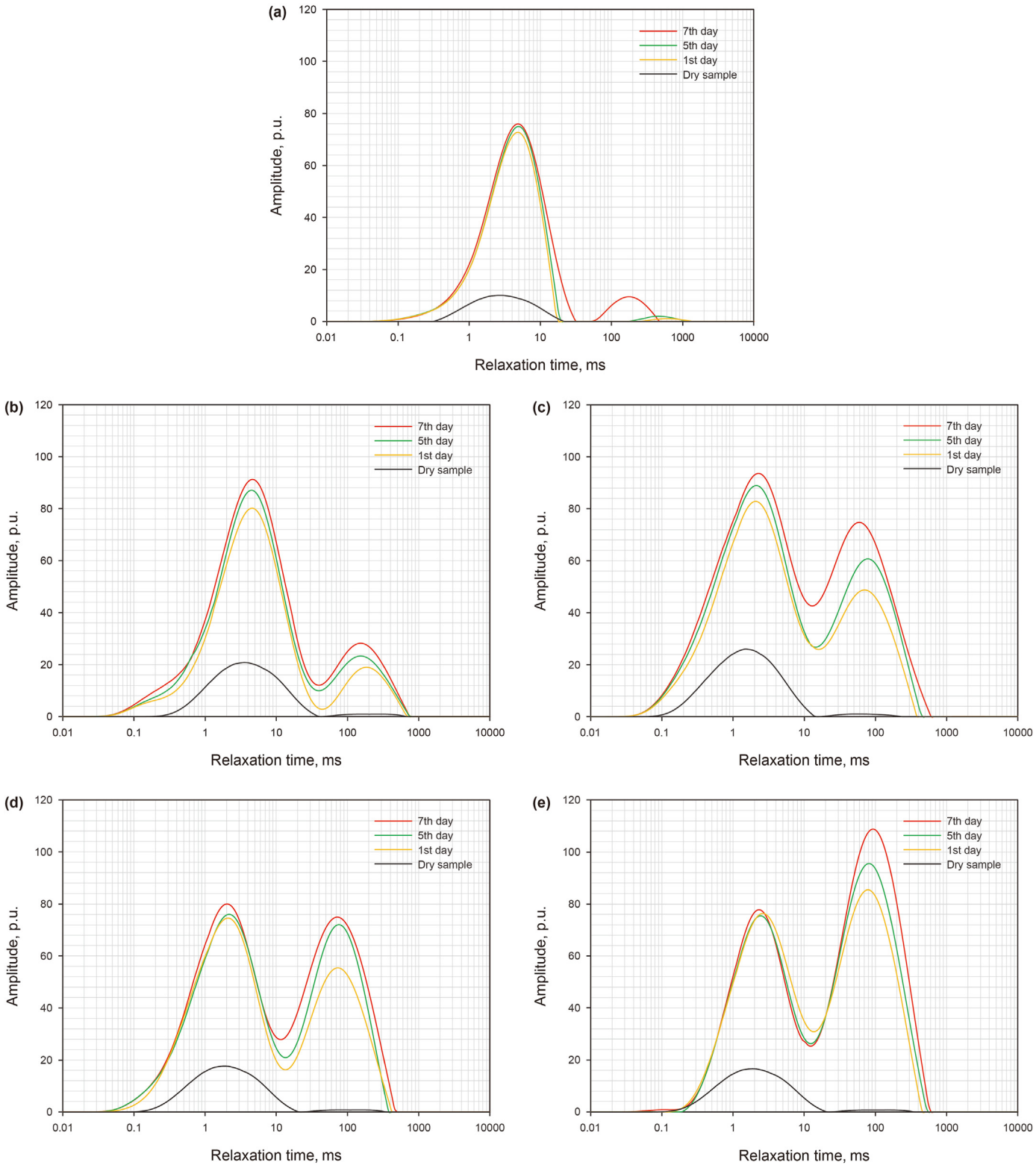

Fig. 8. T_2 spectra of samples with different fracture widths during imbibition stage under 30 MPa. (**a**) Sample with unpropped fracture. Sample with propped fracture width of 0.8 mm **(b)**, 1.0 mm (**c**), 2.0 mm (**d**), and 4.0 mm (**e**).

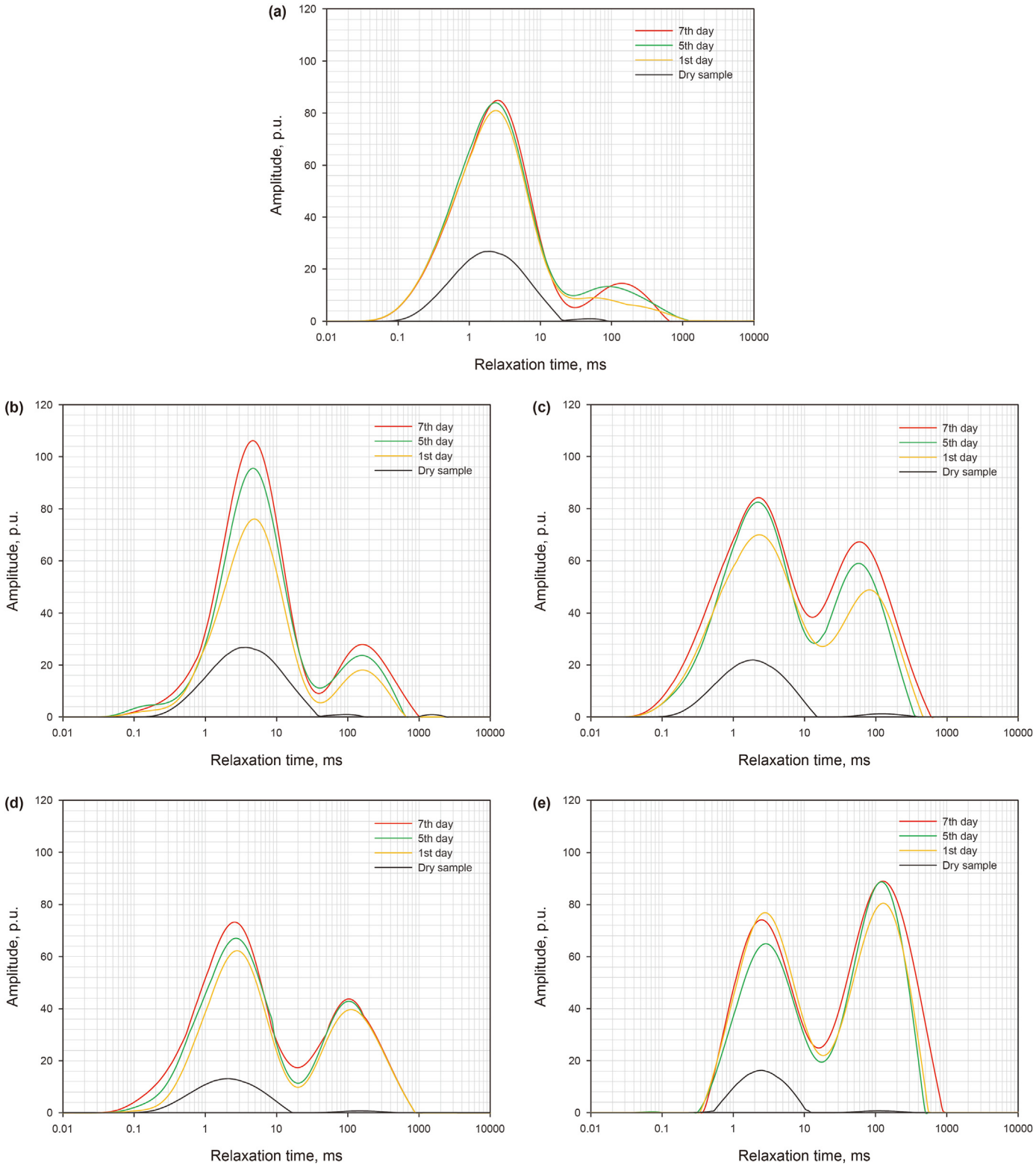

Fig. 9. T_2 spectra of samples with different fracture widths during imbibition stage under 60 MPa. (**a**) Sample with unpropped fracture. Sample with propped fracture width of 0.8 mm **(b)**, 1.0 mm (**c**), 2.0 mm (**d**), and 4.0 mm (**e**).

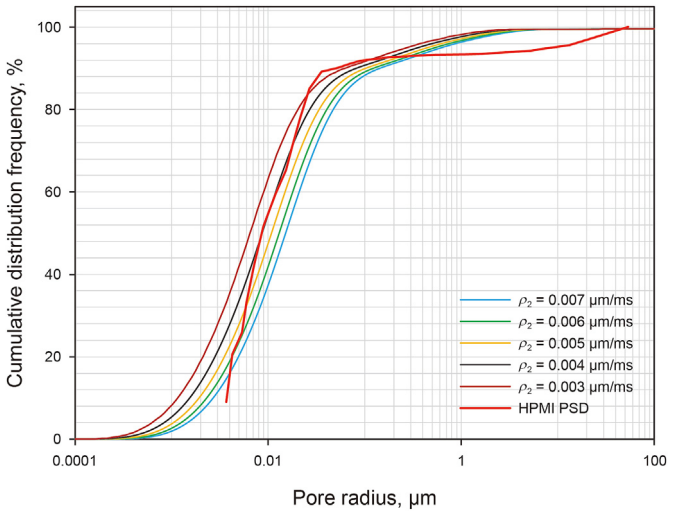

Fig. 10. Surface relaxivity determined by NMR and HPMI measurements.

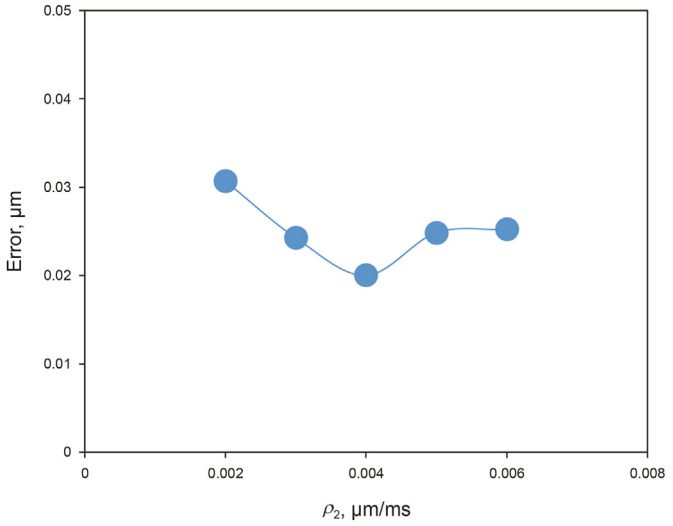

Fig. 11. Error analysis for optimal surface relaxivity.

gas reservoirs.

In addition, the fracture width also has obvious influence on imbibition rate. As shown in Fig. 6(a) and (b), the imbibition rate is positively correlated with the fracture width, especially the initial imbibition rate in Stage I (Fig. 6(b)).

In order to compare experimental results conducted by different researchers and to relate laboratory experiments to reservoir behavior, many scholars have studied the dimensionless treatment method to normalize the imbibition recovery rate and time. Mason et al. (2010) introduced a new viscosity scale factor, and proposed a new dimensionless time incorporating the effects of interfacial tension, fluid viscosity, rock porosity and permeability, core geometry, and boundary condition. The dimensionless time is as follows:

$$t_D = t\sqrt{\frac{k}{\phi}}\cdot\frac{2\sigma}{\mu_w\left(1+\sqrt{\mu_g/\mu_w}\right)}\cdot\frac{1}{L_C^2} \tag{8}$$

where t_D is the dimensionless time; t is the imbibition time, s; k is the gas permeability, mD; σ is the interfacial tension between gas and water, mN/m; ϕ is the core porosity, %; μ_w is the fracturing fluid viscosity measured at 110 °C, which is taken as 0.662 mPa s under 30 MPa, and 0.67 mPa s under 60 MPa; μ_g is the nitrogen viscosity at 110 °C, which is take as 0.0273 mPa s under 30 MPa, and 0.0349 mPa s under 60 MPa; L_C is the feature length, cm. The characteristic length L_C is related to the core size and boundary conditions, which can be calculated as follows:

$$L_C = \sqrt{\frac{V_b}{\sum_{i=1}^{n}\frac{A_i}{S_{A_i}}}} \tag{9}$$

where V_b is the core volume, cm^3; A_i is imbibition area in the direction of i, cm^2; S_{A_i} is the distance from core center to imbibition surface A_i, cm.

Based on the above-mentioned Mason model, the relationships between the normalized imbibition volume and the dimensionless time for samples with different fracture widths are obtained as follows (Fig. 7). The normalized imbibition volume in Fig. 7 is calculated based on the final imbibition volume of each core sample. It can be seen after the normalization, rock samples with different physical properties (i.e., porosity, permeability, and fracture width, propped or unpropped fracture) exhibit similar imbibition dynamics. The imbibition quantity positively correlates with fracture width and pore pressure.

4.3. NMR T_2 spectra during imbibition stage

The distribution of the T_2 spectrum can reflect the distribution of imbibed fracturing fluid in pores of different scales in shale. Fig. 8 shows the T_2 spectra of the shale samples with unpropped fracture and propped fracture. The NMR T_2 spectra of all samples exhibit bimodal distributions with two distinct peaks. The left peak was dominant and located at around 0.01–18 ms, mainly reflecting micropores in the shale matrix. The right peak was lower than the left peak and was located at around 18–666 ms, reflecting medium to large pores in and around fractures.

Different from sandstone, a dry shale sample may generate a basic NMR signal. Hence, the T_2 spectra of dry samples were tested as a benchmark before imbibition. Figs. 8 and 9 show the T_2 spectra of shale samples with fracture widths of 0.8–2 mm under different imbibition pressures. It can be seen that the initial NMR signals of dry samples are unimodal and relatively diminutive. The imbibition effect was most evident on the 1st day of forced imbibition. Due to the higher capillary pressure in small pores, the imbibition volume of small pores was relatively higher. From the 1st day to the 5th day, the imbibition rate of the fracturing fluid slowed down significantly, but the increase in NMR signal of large pores in samples can still be observed during this period. The imbibition rate continued to decrease from the 5th day up to the 7th day, and the T_2 spectrum was stable at the end of the 7th day.

The influence of pressure on the final imbibition volume of large pores was not evident, but the imbibition volume of small pores in the shale samples was significantly affected by pressure. For the shale samples with identical fracture width, the NMR signal measured at the same imbibition time under 60 MPa was larger than that under 30 MPa. In addition, an obvious increase can be observed in the left peak of the T_2 spectra from the 5th day to the 7th day under 60 MPa, indicating that the imbibition effect in the small pores in the shale matrix is highly evident under high pressure.

For shale samples with propped fractures, proppant particles in the fracture form porous media-like pore space under

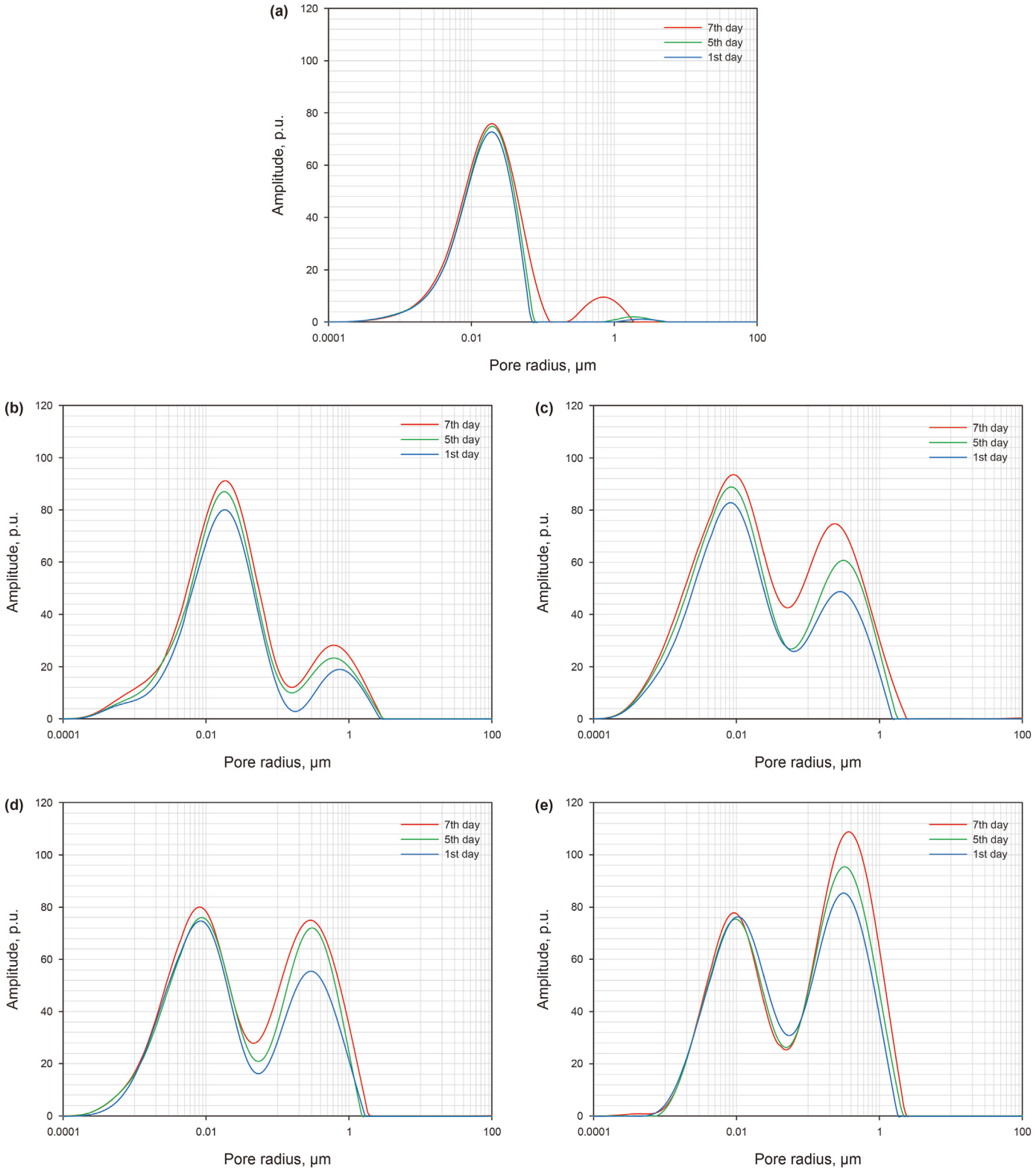

Fig. 12. Pore size distribution of shale samples with different fracture widths under 30 MPa. (**a**) Sample with unpropped fracture. Sample with propped fracture width of 0.8 mm **(b)**, 1.0 mm (**c**), 2.0 mm (**d**), and 4.0 mm (**e**).

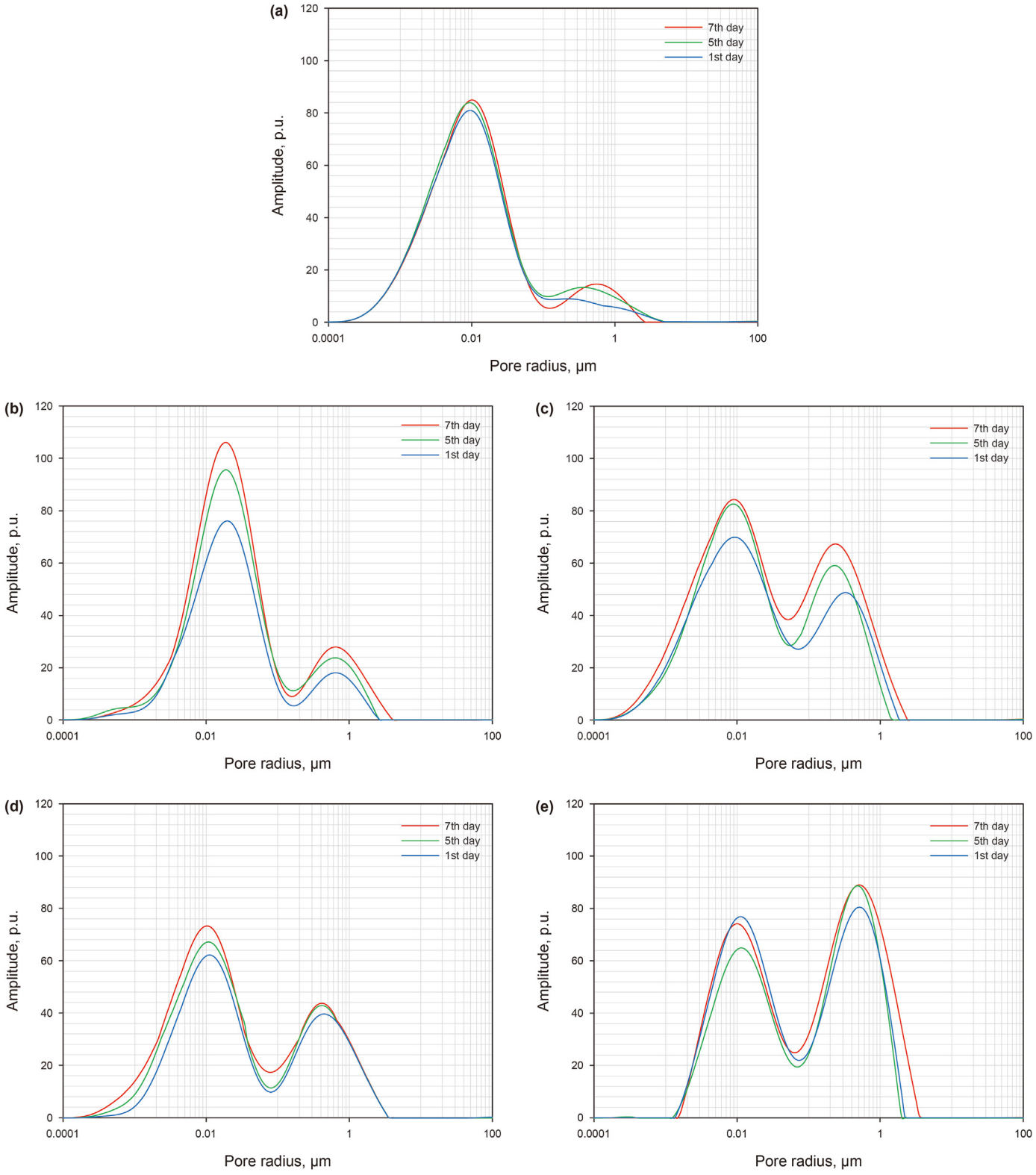

Fig. 13. Pore size distribution of shale samples with different fracture widths under 60 MPa. (**a**) Sample with unpropped fracture. Sample with propped fracture width of 0.8 mm **(b)**, 1.0 mm (**c**), 2.0 mm (**d**), and 4.0 mm (**e**).

Table 5
Pore radius range and cumulative proportion of peaks in T_2 spectra for different shale samples.

Core ID	Fracture width, mm	The 1st day			The 7th day		
		Peak	Radius, μm	Cumulative proportion, %	Peak	Radius, μm	Cumulative proportion, %
I-30-0	0	Left	0.0001–0.062	99.06	Left	0.0001–0.062	93.44
		Right	0.062–4000	0.94	Right	0.062–4000	6.56
I-30-1	0.8	Left	0.0001–0.073	86.77	Left	0.0001–0.073	82.73
		Right	0.073–1600	13.23	Right	0.073–1600	17.27
I-30-2	1	Left	0.0001–0.066	69.55	Left	0.0001–0.066	62.63
		Right	0.066–1445	30.45	Right	0.066–1445	37.37
I-30-3	2	Left	0.0001–0.055	63.08	Left	0.0001–0.055	55.14
		Right	0.055–1201	36.92	Right	0.055–1201	44.86
I-30-4	4	Left	0.0001–0.055	49.53	Left	0.0001–0.055	41.71
		Right	0.055–4000	50.47	Right	0.055–4000	58.29
I-60-0	0	Left	0.0001–0.062	91.52	Left	0.0001–0.062	89.26
		Right	0.062–2762	8.48	Right	0.062–2762	10.74
I-60-1	0.8	Left	0.0001–0.066	80.89	Left	0.0001–0.066	82.08
		Right	0.066–3646	19.11	Right	0.066–3646	17.92
I-60-2	1	Left	0.0001–0.072	67.53	Left	0.0001–0.072	63.64
		Right	0.072–1585	32.47	Right	0.072–1585	36.36
I-60-3	2	Left	0.0001–0.079	62.64	Left	0.0001–0.079	66.97
		Right	0.079–1739	37.36	Right	0.079–1739	33.03
I-60-4	4	Left	0.0001–0.072	51.17	Left	0.0001–0.072	44.45
		Right	0.072–4000	48.83	Right	0.072–4000	55.55

overpressure, which is the main flowing path of shale gas. According to the T_2 spectra of shale samples with different fracture widths under the same pressure, although no specific correlation could be found between imbibition volume and propped fracture width, the total imbibition volume of fracturing fluid generally increased with increasing fracture width.

4.4. Distribution of imbibed fracturing fluid in different scaled pores

In our previous study, we discussed the alteration of NMR T_2 spectra of core samples measured during 7-day high-pressure imbibition. When surface relaxivity ρ_2 in Eq. (4) is determined, the T_2 distribution of different samples can be further converted to pore size distribution (PSD) to quantitatively investigate the distribution of fracturing fluid in different scaled pores under high-pressure imbibition. The relaxivity is usually determined by comparing the NMR T_2 spectra against HPMI data for the same sample.

The HPMI test was conducted at 22.04 °C, the maximum mercury injection pressure is 200.26 MPa, and the minimum mercury injection pressure is 0.0137 MPa. The results of the HPMI test are as follows: the maximum mercury injection saturation is 57.43%, the maximum pore radius is 53.67 μm, the mean pore radius is 16.33 μm, the median saturation pressure is 147.11 MPa, and the uniformity coefficient is 0.306.

Fig. 10 shows the PSD obtained by the HPMI test for a shale sample. It also shows the PSD calculated based on the NMR T_2 spectra with different surface relaxation coefficients for the same sample.

The optimal surface relaxivity is determined when the error between data from NMR and HPMI measurements is minimum. The error function is given as follows (Coates et al., 1999):

$$\delta = \frac{\sqrt{\sum_{i=2}^{n} \omega(x_i)[x_i - w_{x_i}]^2}}{\sqrt{\sum_{i=2}^{n} \omega(x_i)}} \tag{10}$$

where w_{x_i} is the pore size from NMR with assumed surface relaxivities, μm; x_i is the pore size from the HPMI test, μm; $\omega(x_i)$ is the cumulative percentage; and n is the number of HPMI data points. Fig. 11 presents the error corresponding to different surface relaxivities, and it can be observed that the error is minimum when the surface relaxivity is equal to 0.004 ($\rho_2 = 0.004$ μm/ms).

It should be noted that in Fig. 10 the mismatch after 268 nm was caused by different core preparation methods. The core samples for NMR measurements were propped fracture samples, and HPMI measurement needs small piece of shale. So, data based on MRI measurement cannot exactly match those based on HPMI measurement. For the mismatch below 7 nm, it was mainly caused by the limit of the high-pressure mercury injection method which may result in measurement error for micropore distribution.

Once the surface relaxivity was determined, the NMR T_2 spectra of testing core samples can be converted into the PSD. Accordingly, the alterations of imbibed fluid in small pores, large pores and micro-fractures at different imbibition time can be analyzed quantitatively. The pore size distribution occupied by fracturing fluid is shown in Figs. 12 and 13 and Table 5.

For all the fracture samples, the matrix pore and small pore radius ranged from 0.0001 to 0.062 μm, and the large-pore radius ranging 0.062–4000 μm. For the samples with unpropped fractures, micropores predominated the porosity. Matrix porosity accounted for 91.52%–99.06% of total porosity before imbibition and 89.26%–93.44% after imbibition. As the imbibition time increased, obvious fracturing fluid invasion can be observed in different scaled pores in the shale samples, especially in micropores.

4.5. NMR T_2 spectra during migration stage

A large amount of fracturing fluid will still be remained in propped fractures, unpropped fractures and micro-fractures close to the wellbore after fracturing. During the shut-in period after hydraulic fracturing, the remaining fracturing fluid would gradually migrate into matrix pores driven by capillary force and osmotic pressure, causing the shale gas in micropores in the matrix constantly displaced into larger pores or fractures. The gas phase then gradually accumulates and effectively increases the early productivity of the shale gas wells. The redistribution of fracturing fluid in different scaled pores is the so-called migration stage.

Figs. 14 and 15 show the T_2 spectra of shale samples with

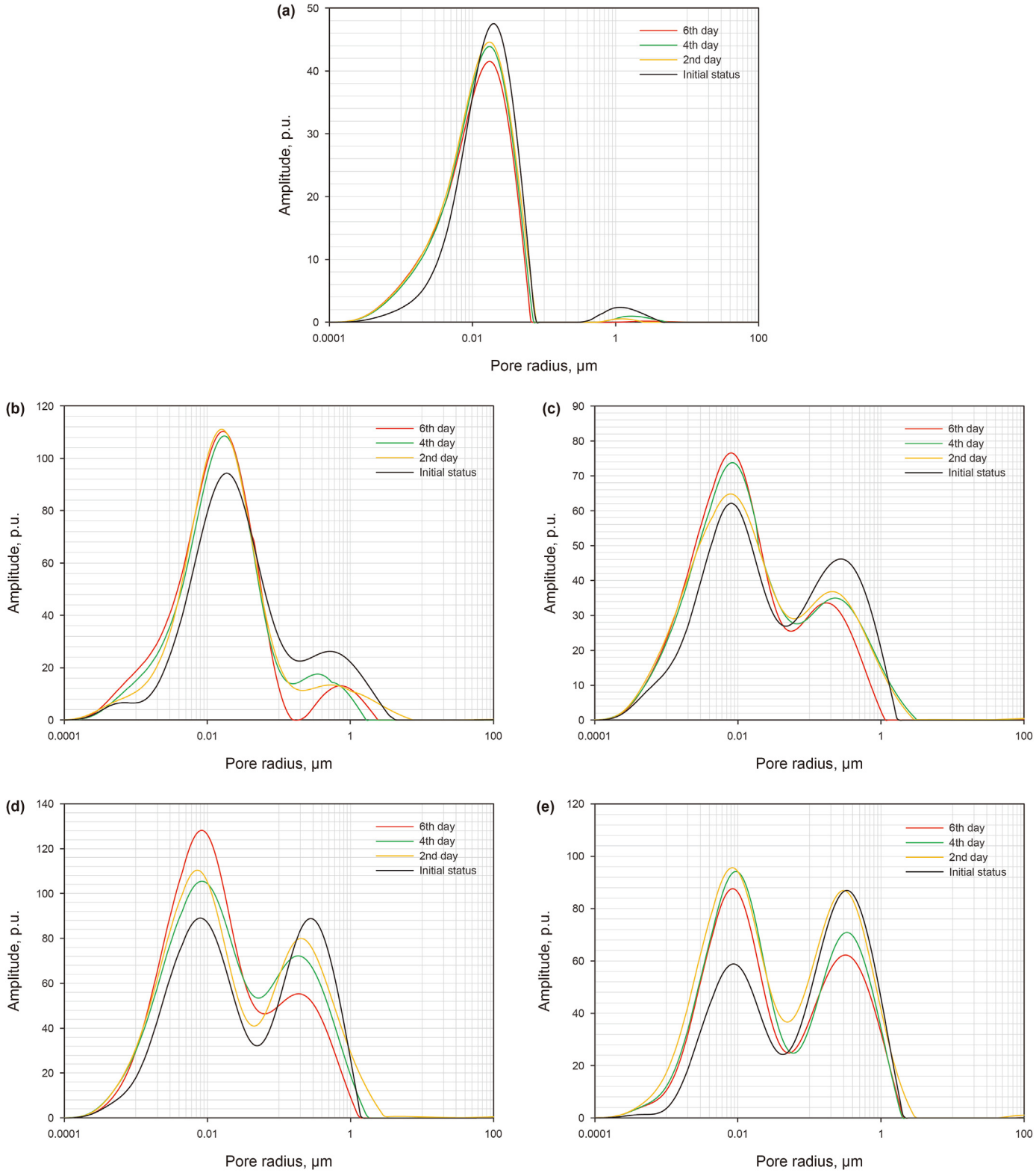

Fig. 14. T_2 spectra of shale samples with different fracture widths during migration stage under 30 MPa. (**a**) Sample with unpropped fracture. Sample with propped fracture width of 0.8 mm (**b**), 1.0 mm (**c**), 2.0 mm (**d**), and 4.0 mm (**e**).

different fracture widths during the migration stage. It can be seen that as the time increased, the left peak of T_2 spectra of all samples increased and the corresponding right peak decreased, reflecting fracturing fluid migrated from large pores into adjacent micropores. As a result, the gas was displaced into the main flowing channels again, and the water blocking in large pores and fractures was relieved to some extent, which may explain the higher productivity of some shale gas wells after soaking period.

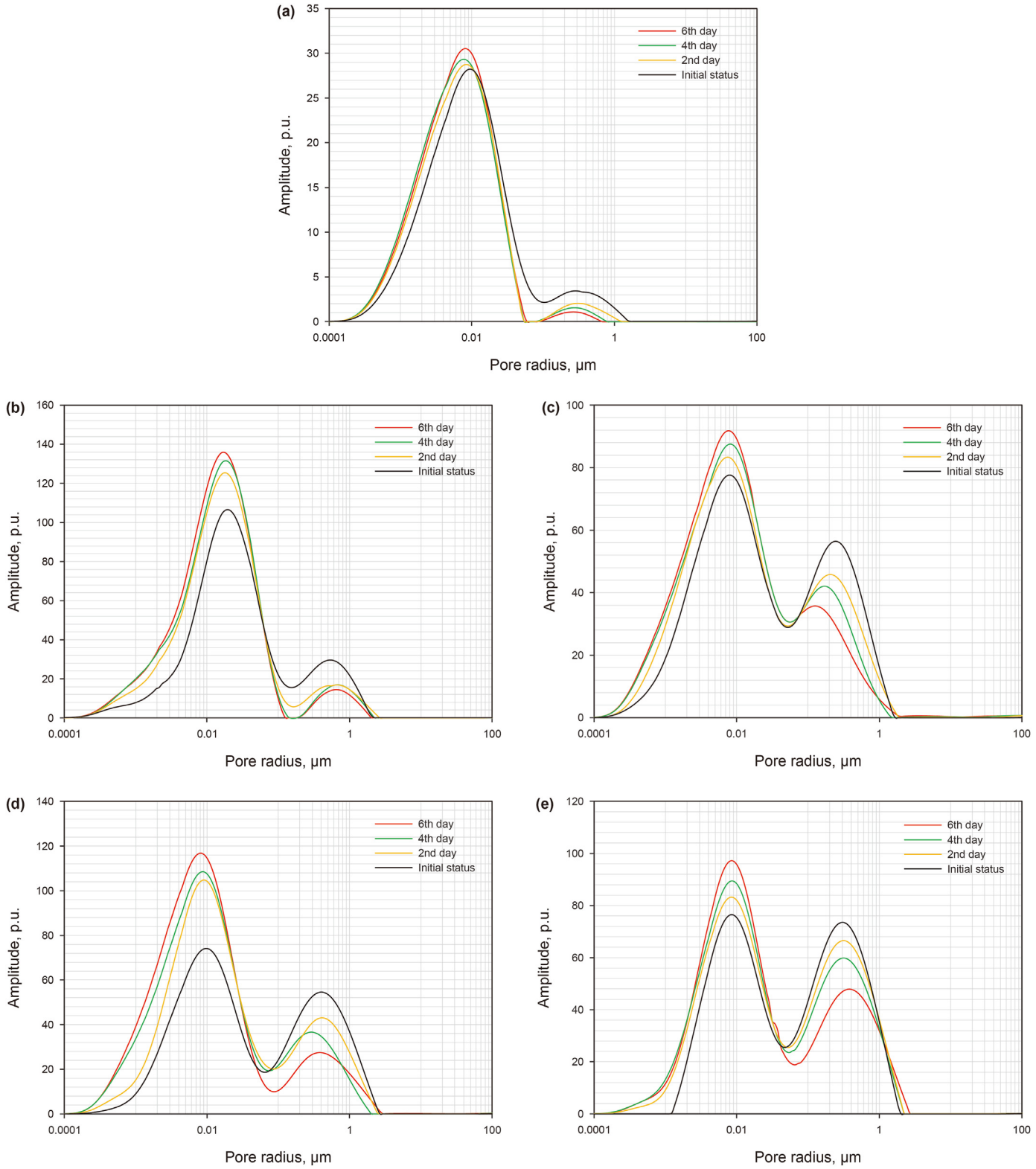

Fig. 15. T_2 spectra of shale samples with different fracture widths during migration stage under 60 MPa. (**a**) Sample with unpropped fracture. Sample with propped fracture width of 0.8 mm (**b**), 1.0 mm (**c**), 2.0 mm (**d**), and 4.0 mm (**e**).

Figs. 16 and 17 present the change of T_2 spectra of shale samples at different migration times. It can be seen that the migration rate gradually decreased with increasing time. In the first two days, the changes in NMR signals of micropores and large pores were obvious. After that, the amplitude of the right peak and the left peak of T_2 spectra still varied but at a much slower rate. In addition, during the whole migration period, fracturing fluid migration was evident in the samples with large fracture width because these

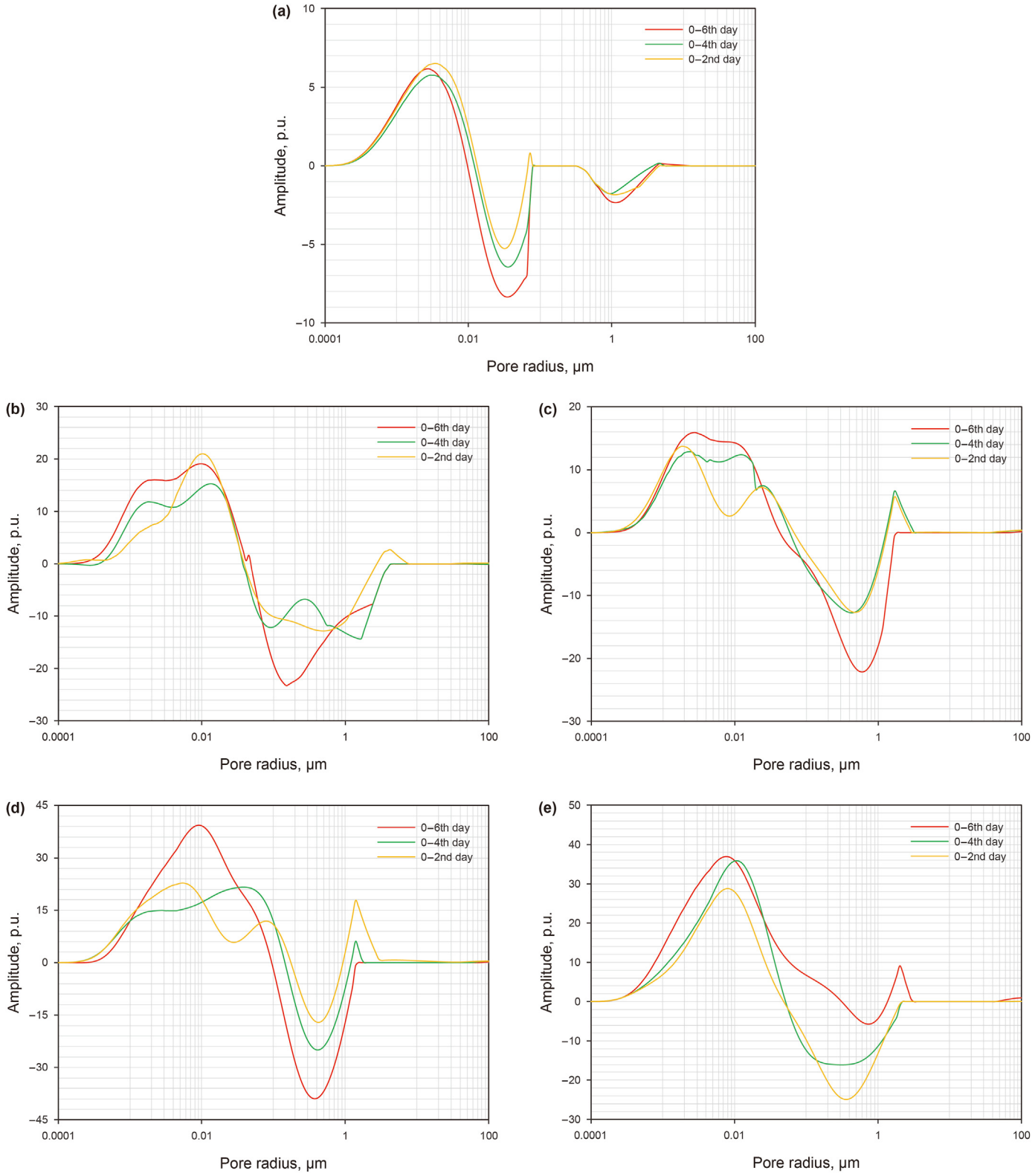

Fig. 16. Changes of T_2 spectra of shale samples with different fracture widths during migration stage under 30 MPa. (**a**) Sample with unpropped fracture. Sample with propped fracture width of 0.8 mm **(b)**, 1.0 mm (**c**), 2.0 mm (**d**), and 4.0 mm (**e**).

samples had more space for storing fracturing fluid. For samples with identical fracture width, the volume of the fracturing fluid migrated into micropores at the same migration time was relatively higher under higher pressure (60 MPa).

4.6. Seepage capacity alteration during migration stage

In this section, the influence of migration (i.e., soaking period) on sample permeability was analyzed. The permeability alterations

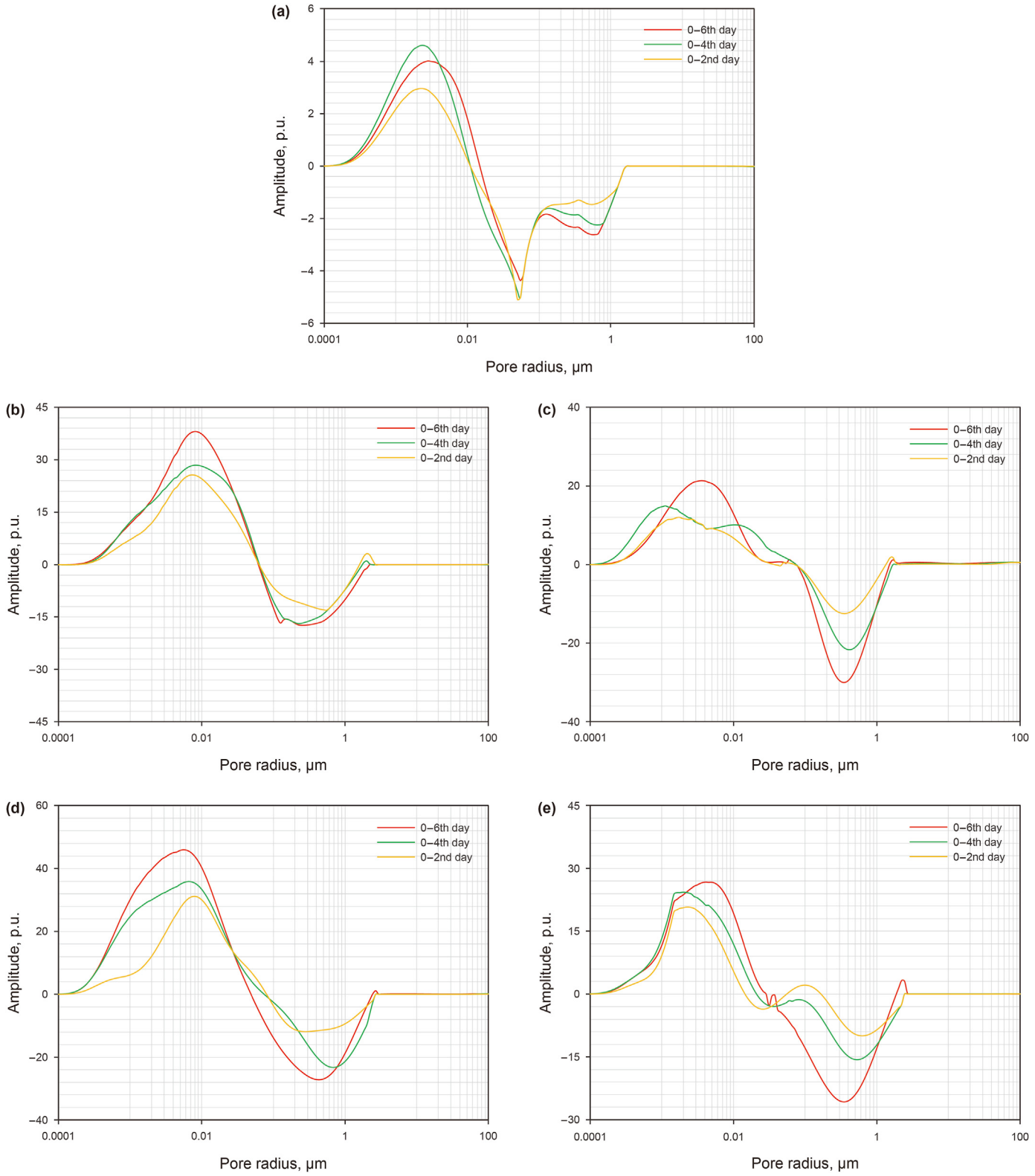

Fig. 17. Changes of T_2 spectra of shale samples with different fracture widths during migration stage under 60 MPa. (**a**) Sample with unpropped fracture. Sample with propped fracture width of 0.8 mm **(b)**, 1.0 mm (**c**), 2.0 mm (**d**), and 4.0 mm (**e**).

for different core samples during migration stage are shown in Fig. 18 and Table 6. It can be observed that compared to the initial gas permeability, the effective gas permeability of rock samples decreased significantly in imbibition stage due to the retention of fracturing fluid. The effective gas permeabilities of all rock samples at the beginning of the migration stage were smaller than 20 mD. The damage ratio of all the core samples ranged between 76.22% and 98.82%, and it increased with increasing fracture width. In

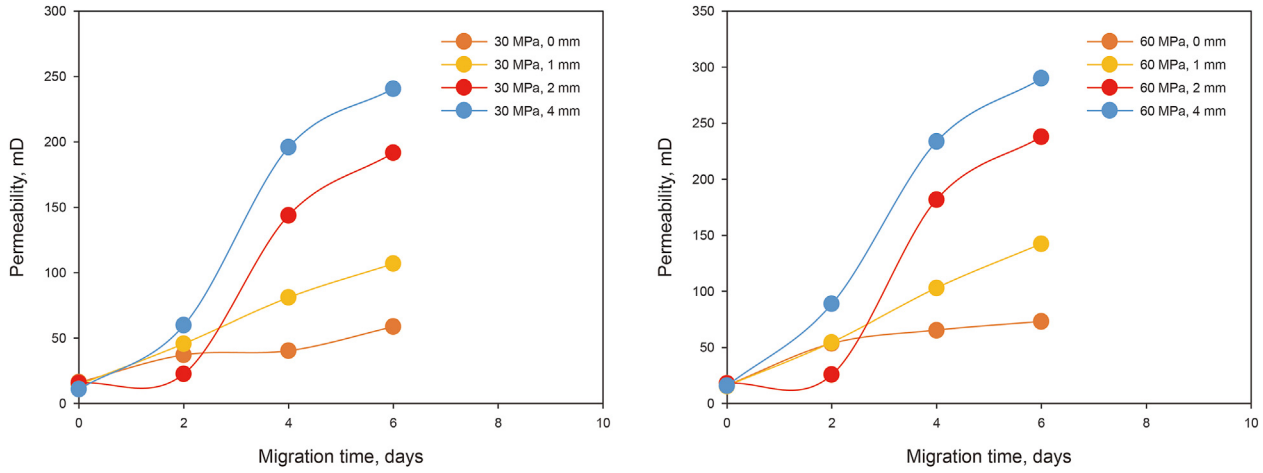

Fig. 18. Permeability alteration during migration stage.

Table 6
Permeability alteration of different samples.

Core ID	Actual width, mm	Permeability, mD					Damage ratio D_k, %	Recovery ratio R_k, %
		Initial K_i	At the beginning of migration K_{g0}	2nd day, K_{g2}	4th day K_{g4}	6th day K_{g6}		
II-30-1	0	68	16.17	37.18	40.40	58.80	76.22	86.48
II-60-1	0	87	16.11	53.53	65.39	73.23	81.69	83.21
II-30-2	0.98	293	14.27	45.70	81.04	106.91	95.13	36.49
II-60-2	1.03	375	15.56	54.55	103.19	142.63	95.85	38.03
II-30-3	1.94	745	15.33	22.56	144.13	191.76	97.94	25.74
II-60-3	2.09	886	18.17	25.76	182.57	237.96	97.95	26.86
II-30-4	3.81	916	10.77	59.89	196.04	240.98	98.82	26.31
II-60-4	3.87	1027	15.77	88.85	233.73	290.10	98.46	28.25

Note: 1) The damage ratio is the gas phase permeability loss caused by the imbibition of fracturing fluid, $D_k = (K_i - K_{g0})/K_i \times 100\%$; 2) The recovery ratio is the degree of the gas phase permeability recovery after six days of migration, $R_k = (K_{g6} - K_{g0})/K_{g0} \times 100\%$.

addition, high pressure would cause more fracturing fluid to imbibe into the matrix, resulting in a decrease in mechanical properties of the fracture surface. Thus, the proppants would be embedded in the fracture surface, which may lead to permeability damage.

During the migration stage, the effective gas permeabilities of all rock samples increase to some extent (25.74%–86.48%). This is because the fracturing fluid would migrate from larger pores into adjacent micropores during soaking, leaving more main flowing channels for gas. It can also be concluded that for samples with propped fractures, the permeability recovery ratio decreases as the fracture width increases, while the experimental pressure has relatively small effect on the permeability recovery ratio. It should be noted that as more and more fracturing fluid imbibing into the matrix, the seepage capacity of shale matrix will inevitably decrease, which is an important reason for the rapid decline of shale gas production.

5. Conclusions

(1) The forced imbibition of shale samples with artificial fractures can be divided into three stages: initial rapid imbibition stage (0–22 h), intermediate transitional imbibition stage (22–48 h), and late stage of stable imbibition (after 48 h). Higher pressure leads to larger imbibition quantity for samples with identical fracture width. As the imbibition pressure increases from 30 to 60 MPa, the increase ratio of the final imbibition quantity of different propped fractures ranges from 15.06% to 32.59%.

(2) The NMR T_2 spectra of all shale samples exhibit bimodal distributions. For the samples with unpropped fractures, micropores predominate the porosity of the shale samples (more than 89.26%). For shale samples with similar fracture width, the difference in the imbibition volume of the fracturing fluid in large pores under different pressures is negligible, but the imbibition quantity of the fracturing fluid in micropores is obviously larger under higher pressure.

(3) Due to the prolonged migration during soaking, the fracturing fluid gradually migrated from artificial fractures or large pores to the adjacent small pores. The shale gas thus was displaced from matrix pores to fractures, and the permeability damage caused by water blocking in propped fractures was relieved. Higher pressure would lead to a larger amount of fracturing fluid diffusing into small pores.

(4) The damage ratio of effective gas permeability of all samples ranges from 76.22% to 98.82% at the end of the imbibition process, and the recovery ratio of effective gas permeability of all samples is between 25.74% and 86.48%. The permeability recovery ratio of the propped samples decreases as the fracture width increases, and the experimental pressure has relatively small effect on the permeability recovery ratio.

Ethical approval

This article does not contain any studies with human participants or animals performed by any of the authors.

Informed consent

Informed consent was obtained from all individual participants included in the study.

Declaration of competing interest

The authors declare that they have no known competing financial interests or personal relationships that could have appeared to influence the work reported in this paper.

Acknowledgements

The authors gratefully acknowledge the support of the National Natural Science Foundation of China (Grant Nos. 52174036, 51774243, 51904257, 51874251), and the Sichuan Province Science and Technology Program (Grant Nos. 2021YJ0345, 2022JDJQ0009, 2022NSFSC0186).

References

Bazin, B., Peysson, Y., Lamy, F., et al., 2010. In-situ water-blocking measurements and interpretation related to fracturing operations in tight gas reservoirs. SPE J. 25 (4), 431–437. https://doi.org/10.2118/121812-PA.

Bennion, D.B., Thomas, F.B., Bietz, R.F., et al., 1996. Water and hydrocarbon phase trapping in porous media-diagnosis, prevention and treatment. J. Can. Petrol. Technol. 35 (10), 29–36. https://doi.org/10.2118/96-10-02.

Bostrom, N., Chertov, M., Pagels, M., et al., 2014. The time-dependent permeability damage caused by fracture fluid. In: SPE International Symposium and Exhibition on Formation Damage Control. https://doi.org/10.2118/168140-MS.

Cai, J., 2021. Some key issues and thoughts on spontaneous imbibition in porous media. Chin. J. Comput. Phys. 38 (5), 505–512 (in Chinese).

Chen, H., Zhou, T., Fan, H., et al., 2020. Preparation method and stress sensitivity of core samples with hydraulic fractures in shale reservoirs. Acta Pet. Sin. 41 (9), 1117–1126 (in Chinese).

Cheng, Y., 2012. Impact of water dynamics in fractures on the performance of hydraulically fractured wells in gas-shale reservoirs. SPE J. 51 (2), 143–151. https://doi.org/10.2118/127863-PA.

Cluff, R.M., Byrnes, A.P., 2010. Relative permeability in tight gas sandstone reservoirs - the "permeability jail" model. In: SPWLA 51st Annual Logging Symposium. Society of Petrophysicists and Well-Log Analysts.

Coates, G.R., Xiao, L., Prammer, M.G., 1999. NMR Logging: Principles and Applications. Gulf Publishing Company, Texas.

Dutta, R., Lee, C.-H., Odumabo, S., et al., 2014. Experimental investigation of fracturing-fluid migration caused by spontaneous imbibition in fractured low-permeability sands. SPE J. 17 (1), 74–81. https://doi.org/10.2118/154939-PA.

Gao, S., Hu, Z., Guo, W., et al., 2013. Water absorption characteristics of gas shale and the fracturing fluid flowback capacity. Nat. Gas. Ind. (12), 71–76 (in Chinese).

Ghanbari, E., Dehghanpour, H., 2015. Impact of rock fabric on water imbibition and salt diffusion in gas shales. Int. J. Coal Geol. 138 (4), 55–67. https://doi.org/10.1016/j.coal.2014.11.003.

Handy, L., 1960. Determination of effective capillary pressures for porous media from imbibition data. Trans. AIME 219 (1), 75–80. https://doi.org/10.2118/1361-G.

Liu, D., 2017. Research on Microcosmic Laws of Fracture Fluid Imbibition and Mechanisms of Productivity Enhancement by "Shut-in" in Unconventional Hydrocarbon Reservoir. Master Thesis. China University of Petroleum, Beijing, China (in Chinese).

Liu, Z., Liu, D., Cai, Y., et al., 2020. Application of nuclear magnetic resonance (NMR) in coalbed methane and shale reservoirs: a review. Int. J. Coal Geol. 218, 103261. https://doi.org/10.1016/j.coal.2019.103261.

Lucas, R., 1918. Rate of capillary ascension of liquids. Kolloid Z. 23 (1), 15–22.

Mianmo, M., Hongkui, G., Wenming, J., et al., 2015. Monitor the process of shale spontaneous imbibition in co-current and counter-current displacing gas by using low field nuclear magnetic resonance method. J. Nat. Gas Sci. Eng. 27 (1), 336–345. https://doi.org/10.1016/j.jngse.2015.08.069.

Mason, G., Fischer, H., Morrow, N.R., et al., 2010. Correlation for the effect of fluid viscosities on countercurrent spontaneous imbibition. J. Pet. Sci. Eng. 72 (1–2), 195–205. https://doi.org/10.1016/j.petrol.2010.03.017.

Roshan, H., Ehsani, S., Marjo, C., et al., 2015. Mechanisms of water adsorption into partially saturated fractured shales: an experimental study. Fuel 159 (3), 628–637. https://doi.org/10.1016/j.fuel.2015.07.015.

Saidian, M., Prasad, M., 2015. Effect of mineralogy on nuclear magnetic resonance surface relaxivity: a case study of Middle Bakken and Three Forks formations. Fuel 161, 197–206. https://doi.org/10.1016/j.fuel.2015.08.014.

Shen, Y., Ge, H., Su, S., et al., 2017. Imbibition dynamic characteristics and water locking potential of shale gas reservoir. Scientia Sinica Physica, Mechanica & Astronomica. 47 (11), 84–94. https://doi.org/10.1360/SSPMA2016-00538 (in Chinese).

Sherman, J.B., Holditch, S.A., 1991. Effect of injected fracture fluids and operating procedures on ultimate gas recovery. In: SPE Gas Technology Symposium. https://doi.org/10.2118/21496-MS.

Terzaghi, K., 1943. Theoretical Soil Mechanics. John Wiley & Sons, Inc, Hoboken. https://doi.org/10.1002/9780470172766.

Wang, J., Rahman, S.S., 2015. An investigation of fluid leak-off due to osmotic and capillary effects and its impact on micro-fracture generation during hydraulic fracturing stimulation of gas shale. In: EUROPEC 2015. https://doi.org/10.2118/174392-MS.

Washburn, E.W., 1921. The dynamics of capillary flow. Phys. Rev. J. 17 (3), 273–283. https://doi.org/10.1103/PhysRev.17.273.

Xia, Y., Tian, Z., Xu, S., et al., 2021. Effects of microstructural and petrophysical properties on spontaneous imbibition in tight sandstone reservoirs. J. Nat. Gas Sci. Eng. 96, 104225. https://doi.org/10.1016/j.jngse.2021.104225.

Yang, L., Ge, H., Shi, X., et al., 2017. Experimental and numerical study on the relationship between water imbibition and salt ion diffusion in fractured shale reservoirs. J. Nat. Gas Sci. Eng. 38 (1), 283–297. https://doi.org/10.1016/j.jngse.2016.12.010.

Zeng, Y., Pang, Y., Ding, S., et al., 2022. Pore-fracture network alteration during forced and spontaneous imbibition processes in shale formation. J. Petrol. Sci. Eng. 209, 109846. https://doi.org/10.1016/j.petrol.2021.109846.

Zhu, Y., Li, Z., 2021. Imbibition behavior and fluid dynamic distribution of Longmaxi formation shale in Pengshui area. Chin. J. Comput. Phys. 38 (5), 555–564 (in Chinese).

Zou, C., Zhao, Q., Cong, L., et al., 2021. Development progress, potential and prospect of shale gas in China. Nat. Gas. Ind. 41 (1), 1–14 (in Chinese).